Experimental Study on the Turbulent Flow Field inside Hydrocyclone with Particle Image Velocimetry

Xu Duan*
TSI Instrument (Beijing) Co., Ltd, Beijing, China

Keywords: Particle Image Velocimetry (PIV), Turbulent flow field, Axial velocity, Radial velocity, Secondary vortexes

Abstract: The hydrocyclone separation is highly related to its flow field. The investigation of the turbulent flow characteristics helps the optimization of the hydrocyclone structure design. In this article, the turbulent flow field in a 50mm hydrocyclone was investigated with Particle Image Velocimetry. The cylinder section and part of the cone section are measured simultaneously. Both the axial and radial velocity components peak in the central area of the hydrocyclone. But for radial velocity, it varies between inward and outward from top to bottom, not exclusively inward in the cone section. The secondary vortexes exist in the transition area of inner spiral flow and outer spiral flow, where higher vorticity is located. Turbulent intensity and Reynolds shear stress is calculated from the two velocity components with time series. It has been made clear that the central area is where the turbulence is strongest. And the maximum radial turbulence intensity exists in the vicinity of vortex finder tip, while maximum axial turbulence intensity exists in the lower cone section with transition of flow. Results show the averaged velocity field is smoother and more convenient for comprehending while the instantaneous velocity field is less distorted by the averaging process.

1 INTRODUCTION

Hydrocyclone has been widely used for its simplicity in manufacturing and efficiency in long-term running. But the flow field, which explains how the separation is working, is more complicated to make clear.

The difficulties should be attributed to the turbulent and three-dimensional characteristics. Previous works mostly relied on Laser Doppler Velocimetry (LDV) or Phase Doppler Particle Analyzer (PDPA) measurements (Bergstrom & Vomhoff, 2007), which only measured the two or three components of velocity in a single point. Since the measurement of points is not conducted simultaneously, it becomes problematic to discuss the instantaneous velocity profile. The PDPA results were sampled by hundreds or even thousands of single-point data of velocity components in one interval of time. Most previous works on hydrocyclonic flow field measurements with PDPA were displaying averaged velocity profile (Yang et al., 2011). Of course, some researchers did present some turbulence information, such as RMS value (Zhang et al., 2009). But data is restricted in a certain vertical position and it's impossible to have an overall view on the hydrocyclone flow field. Another problem is the measurement of radial velocity. The ordinary configuration of PDPA is only able to measure the tangential and axial velocity. Even though the 3D PDPA has been developed recently, the relatively lower value of radial velocity makes it even more difficult to get convincing conclusion.

Although Particle Image Velocimetry (PIV) is a common and mature measurement method, its application in hydrocyclone measurement is rare. In fact, PIV is very suitable to measure the velocity field inside hydrocyclone, especially the turbulent feature and the specific features such as secondary vortexes. Marins et al. (2010) measured the velocity field in a hydrocyclone with both LDA (similar to PDPA) and PIV, but the area of interest for PIV is in a 1° cone near underflow, where the hydrocyclone wall is thin enough. And he discussed the turbulence data based on LDA measurement. Lim et al. (2010) measured both cylindrical section and cone section with PIV, but he used it mainly for the validation of CFD result and didn't draw impressive conclusions. Little literature focused on the hydrocyclone flow field measurement with PIV, but some research on gas cyclone measurement is inspiring. Zheng and

Duan, X.
Experimental Study on the Turbulent Flow Field inside Hydrocyclone with Particle Image Velocimetry.
In *Proceedings of the 7th International Conference on Water Resource and Environment (WRE 2021)*, pages 219-225
ISBN: 978-989-758-560-9; ISSN: 1755-1315

Wong made a comprehensive studied on a gas cyclone (Zheng et al., 2006; Wong et al., 2007). He divided the cyclone into three sections and measured separately. The problem is that the sections were not connected and not measured simultaneously. This means the loss of some specific features of secondary vortexes throughout the cross-section.

In this article, the flow field inside an optical glass 50mm hydrocyclone was measured with Particle Image Velocimetry (PIV). The instantaneous velocity profile and vorticity profile is presented and made comparison with their average counterparts. The other turbulent information, such as turbulent intensity and Reynolds shear stress are also discussed.

2 EXPERIMENTAL

2.1 Hydrocyclone Model

The geometry of Φ50mm hydrocyclone for PIV test is shown in Figure 1 and the detailed parameter is in table 1. This type of hydrocyclone in is mainly designed for solid-liquid separation, for example, the Methanel to Olefin (MTO) quench water treatment. Optical grade fused quartz (JGS2) was chosen as the material of the cyclone body, for considering its good UV and visible transmission. The optical grade fused quartz is relatively low for refractive index, which make it suitable for image measurement methods.

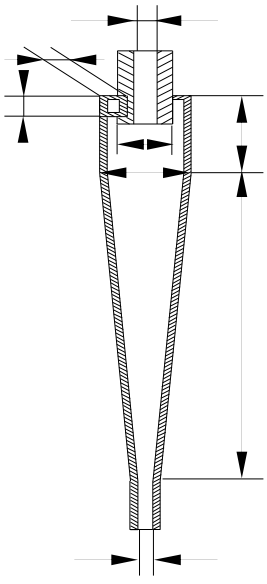

Figure 1: The geometry of hydrocyclone.

Table 1: Dimensions of the hydrocyclone.

D/mm	50
L1/D	1.48
L2/D	8.78
do/D	0.24
Do/D	0.68
du/D	0.08
d/mm	8
h/mm	12

2.2 Experimental Setup

2.2.1 Experimental Procedure

As is shown in Figure 2, water was pumped from a 50L tank to a buffer vessel for a smoother pressure profile, and then into the hydrocyclone through the rectangular tangential inlet. Both the overflow and the underflow went back to the tank to complete a circulation of the feed material. Hollow glass microspheres were seeded to trace the fluid flow. The medium size of the tracer particles is around 10μm, while their particle density is about 1100g/cm3. Three pressure gauges were fixed on all the inlet and outlets to determine the feed pressure and control the split ratio. To eliminate the distortion created by the phenomenon of refraction, we introduced an index matching method for the acquisition of images with improved quality. The hydrocyclone is put inside a rectangular PMMA box and filled with water inside and outside the hydrocyclone. Thus, the distortion of image was minimized for a better result.

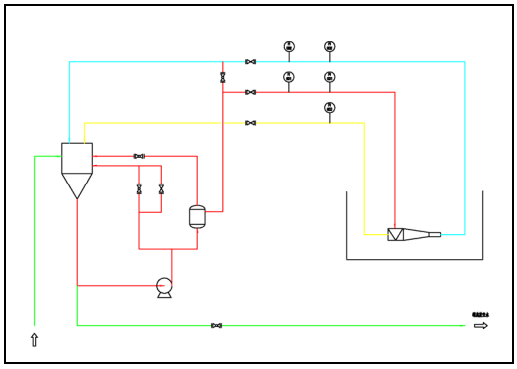

Figure 2: Experimental setup.

Table 2: Instrumentation.

Setup	Model	Parameter of Apparatus		Manufacturers
Nd:YAG Laser	Vlite-500	Wavelength	532 nm	Beamtech
		Energy	500 mJ/Pulse	
		Pulse Duration	6-8 ns	
		Repetition Rate	15 Hz	
		Beam Size	8 mm	
		Timing Jitter	2 ns	
Synchronizer	610035	Delay	0-1000s	TSI
		Pulsewidth	10ns-1000s	
		Resolution	1ns	
		Jitter	<400ps	
CCD Camera	630159	Pixel Resolution	400,82,672pixels	TSI
		Frame Rate	15 fps	
		Frame Straddling Time	200ns	
		Camera Lens	60mm	Nikon

2.2.2 Instruments for Measurement

The particle image is captured with a TSI 630159 CCD system. To get images with better quality, a Nikon 60mm micro-lens is mounted to the TSI camera. The light sheet is created with the combination of cylindrical lens and spherical lens. The two lenses are mounted in the front of laser emitter of the light arm, which guides the light from the laser device. The detailed components of instrumentation are shown in Table 2. Figure 3 show the measurement instruments of hydrocyclone for PIV test.

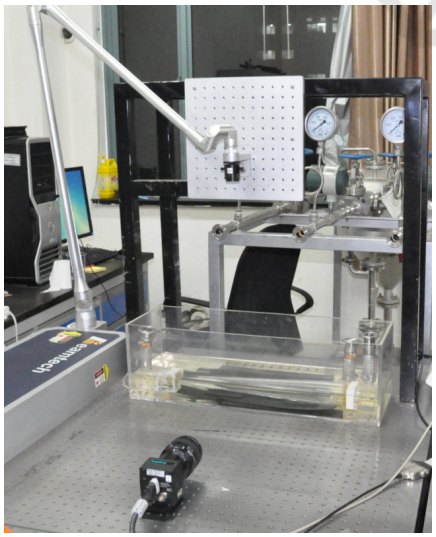

Figure 3: The measurement instruments.

3 RESULTS AND DISCUSSION

3.1 The Axial Velocity Profile

In this experiment, the flow inside hydrocyclone is operated to a quasi-stable state with no air-core. A set of two particle images of the central plane orthogonal to the inlet are captured instantaneously. The capture interval Δt between the two images of one straddle is set to 100μs and the exposure time is 300μs. The PIV measurement of flow field inside hydrocyclone is repeated by 200 times to obtain an averaged velocity profile.

Figure 4 shows the axial velocity with the Locus of Zero Vertical Velocity (LZVV) with the inlet pressure at 50kpa, 100kpa and 150kpa. It can be seen that the upward axial velocity magnitude peaks in the central area. The downward axial velocity peaks in the vicinity of the hydrocyclone wall. The axial velocity in the area around the LZVV is very slight in value, where the primary flow will stay longer inside the hydrocyclone before discharged from the underflow orifice or overflow pipe. The locus divides the hydrocyclone into two areas: one promoting the separation process (with downward axial velcoity) and the other detrimental. From the three axial velocity contour maps under different inlet pressure, the LZVV are in the same shape for similar split ratio of the hydrocyclone. And the locus is located around 1/6 radius of the cylinder section away from the hydrocyclone wall.

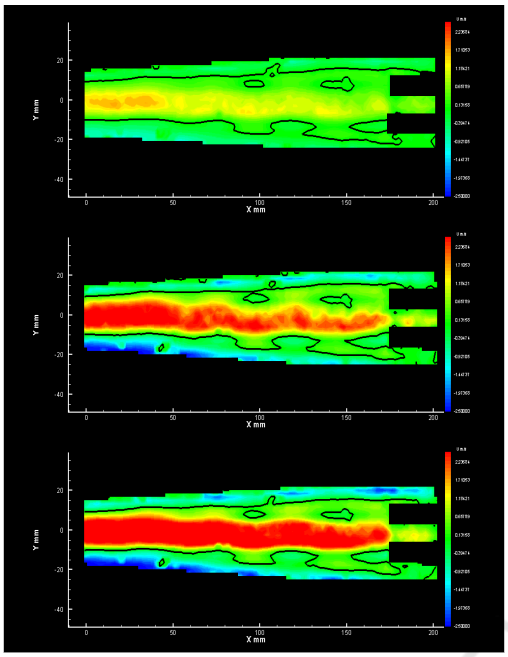

Figure 4: The axial velocity contour. contoury (LZVV)tantaneous vector map of hydrocyclone flow filed.

3.2 The Radial Velocity Profile

Figure 5 shows the radial velocity profile with the inlet pressure at 50kpa, 100kpa and 150kpa. The radial velocity is asymmetric even in absolute value. The asymmetric in absolute value may be attributed to the single injection of flow. It's obvious that the radial velocity peaks in the area very close to the axis. The peak radial velocity is around 20% of the axial flow. Although the hydrocyclone is operated without an air-core, there still exist some upward flows in the central area with little radial movement.

Another feature of the radial velocity profile is its variation along axis. It is of great difference from axial velocity component (or tangential velocity component) that the radial velocity varies sharply between outward direction and inward direction. But most former researchers reported inward velocity in the cone section, depending on their PDPA measurements (Bergstrom & Vomhoff, 2007). And Luo et al. (1989) concluded it with an equation shown as following:

$$v_r r^m = -c$$

It was the single-point feature of measurements with PDPA that resulted in this misunderstanding. The radial velocity is more complicated than it was previously deemed. It was clear with PIV measurements hat the radial velocity is inward in the upper cone section in only one half of the hydrocyclone. As a matter of fact, except for the limited area near hydrocyclone wall, the inward radial velocity will be replaced by outward radial velocity in the lower cone section. And the radial velocity profile is just the opposite in the other side of the axis. As to the inward radial velocity profile along axial direction in cone section, it will increase to the maximum and then decrease to zero and finally replaced by outward velocity. Thus, the radial velocity equation should be modified to satisfy this situation. We can keep the assumption that the radial velocity followed the similar regulation of tangential velocity in the inward region. But for the outward region, the constant $-c$ should be positive. What's more, it is obvious that the constant m and C should be changing along axial direction.

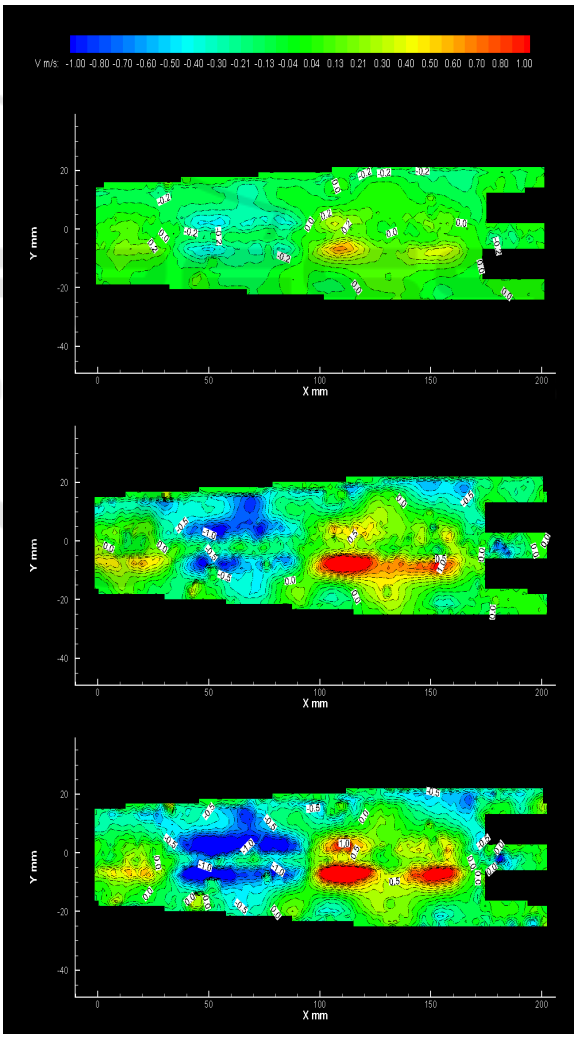

Figure 5: The radial velocity contour.

3.3 The Two-dimensional Velocity and Vorticity Profile

The averaged two-dimensional two-component (2D2C) velocity profile is shown in Figure 6(a).

For the three visualizations of hydrocyclonic flow field with the inlet pressure at 50kpa, 100kpa and 150kpa, the vector maps are very similar for the structure, but the velocity magnitude increases with increasing inlet pressure. The peak values of velocity magnitude of all the three visualizations are located in the central axis of the hydrocyclone. The velocity vectors are pointed downward near wall and upward near the axis. This information gives a general idea for the averaged two-dimensional two-component (2D2C) velocity profile.

Another significance of the 2D2C velocity profile is the identification of secondary vortexes. Figure 7(a) shows the diagram of streamlines imposed on the vorticity contour. It can be seen that the vortexes are distributed between the central axis. The vortexes are in the same rotation sense when located in the same half, denoting similar formation mechanism. The secondary vortexes are long recognized as the "mantle" which is detrimental to particle transportation from axis to wall. Although the influence of secondary vortexes is not clear so far, it's worth paying attention to its characteristics.

The vorticity distribution profile also denotes the rotation sense. The Z vorticity $\vec{\omega}$ that is presented in Figure 6 represents the degree of local fluid rotation and valuable for the determination of the vortex characteristic and turbulence. The Z vorticity $\vec{\omega}$ is calculated with the following equation:

$$\vec{\omega} = \nabla \times \vec{v} = (\frac{\partial}{\partial x}, \frac{\partial}{\partial y}) \times (v_x, v_y) = \frac{\partial v_x}{\partial x} - \frac{\partial v_y}{\partial y}$$

The relatively higher vorticity is located in the transition area of inner spiral flow and outer spiral flow. The location is also where secondary vortexes exist, mainly owing to the sharp transition of the primary flow. The local rotation of fluid would influence a lot to the particle behavior. If consider a group of particle transporting from axis to wall and experiencing a secondary vortex, the particles will inevitable rotate by themselves and the mass transfer process will be enhanced.

In comparison with the instantaneous velocity vector map in Figure 6(b), the averaged velocity profile is smoother and more convenient for comprehending. But in another hand, the instantaneous velocity profile is not distorted by the averaging process. The instantaneous streamline superimposed on the vorticity contour map (with the inlet pressure at 100kpa) is presented in Figure 7(b). We found some extra secondary vortexes in the instantaneous map. This indicates that in the turbulent flow field inside hydrocyclone, the large-scale secondary vortexes are not able to keep always stable, and they will break up to form several smaller scale vortexes. The comparison of the two streamline diagrams also demonstrates that the averaging process will eliminate some detailed structures in the flow field.

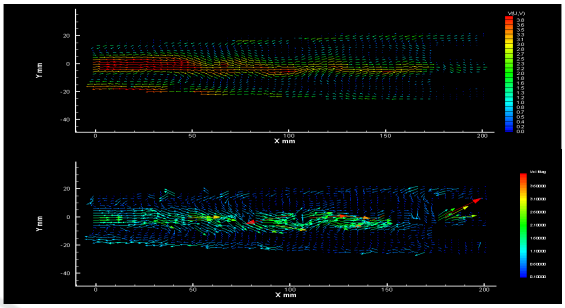

Figure 6: Averaged and instantaneous vector map of hydrocyclone velocity field.

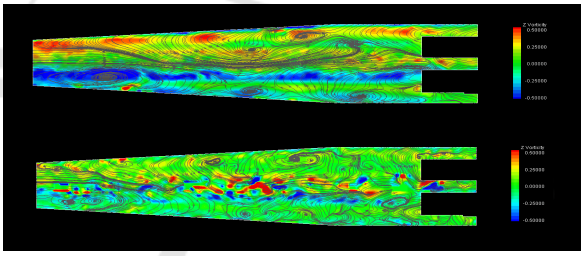

Figure 7: Typical streamline superimposed on the vorticity distribution contour map.

3.4 The Turbulent Intensity

Figure 8 and Figure 9 shows the standard deviation of axial velocity and radial velocity, respectively. The standard deviation is calculated from the 200 visualizations of the velocity field inside hydrocyclone. The standard deviation σ for axial velocity and radial velocity are defined by the following equations:

$$\sigma_u = \sqrt{\frac{\sum u_i'^2}{n}} = \sqrt{\frac{(u_1 - \bar{u})^2 + (u_2 - \bar{u})^2 + \ldots + (u_i - \bar{u})^2}{n}}$$

i=1,2,…,n

$$\sigma_v = \sqrt{\frac{\sum v_i'^2}{n}} = \sqrt{\frac{(v_1 - \bar{v})^2 + (v_2 - v)^2 + \ldots + (v_i - \bar{v})^2}{n}}$$

i=1,2,…,n

The standard deviation σ is also called the turbulent intensity, representing the degree of velocity variation in the turbulent flow. Its square is the same with non-normalized Reynolds normal stress. In Figure 7, the standard deviation of axial velocity is rather slight at the quasi-free vortex area. The turbulence there is not so strong in comparison to that in the forced vortex area. And the relatively higher axial velocity in the forced vortex area also contributes a lot to this phenomenon.

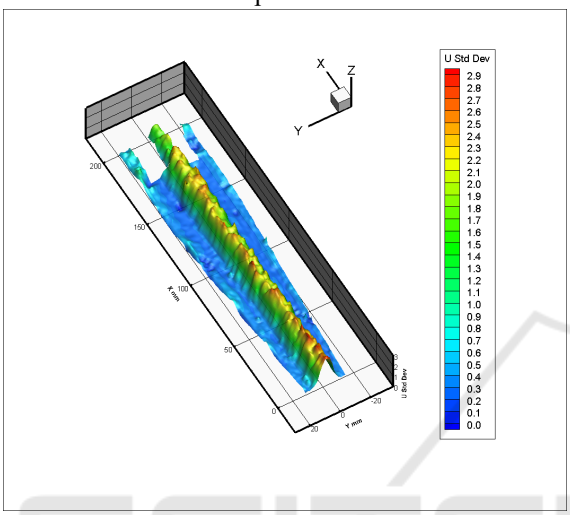

Figure 8: The standard deviation of axial velocity.

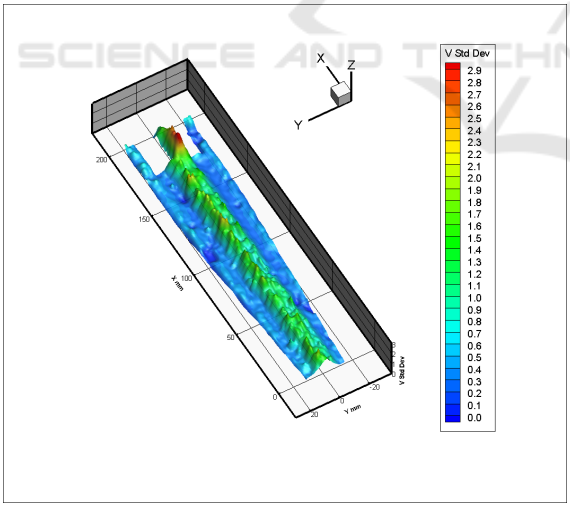

Figure 9: The standard deviation of radial velocity.

As is shown in Figure 8, the standard deviation of axial velocity is also higher in the forced vortex area. But it peaks in the vicinity of the vortex finder, while the standard deviation of axial velocity peaks in the lower part of the cone section. Experimental results show the radial velocity in the vicinity of the vortex finder is not so high, which indicates the turbulence there is rather strong. This reminds us to modify the vortex finder shape or size to reduce the turbulence and minimize the bad influence of back-mixing in some classification process.

3.5 The Reynolds Shear Stress

The Reynolds shear stress is the index for turbulent fluctuations in fluid momentum. It is obtained from the averaging process over the Navier-Stokes equations and defined by the following equation:

$$\tau_{ij}^{''} = \overline{u_i' v_j'} = \frac{\sum (u_i - \bar{u})(v_j - \bar{v})}{n} \qquad \text{i=1,2,…,n; j=1,2,…,n}$$

Figure 10 shows the Reynolds shear stress in the surface. It is found that the much higher Reynolds shear stresses are produced in the central area. The lower values are found in the vicinity of hydrocyclone wall. It demonstrates again the central area of the hydrocyclone is where the turbulence concentrates. The data of Reynolds stress could also serve as the reference for model validation and modification.

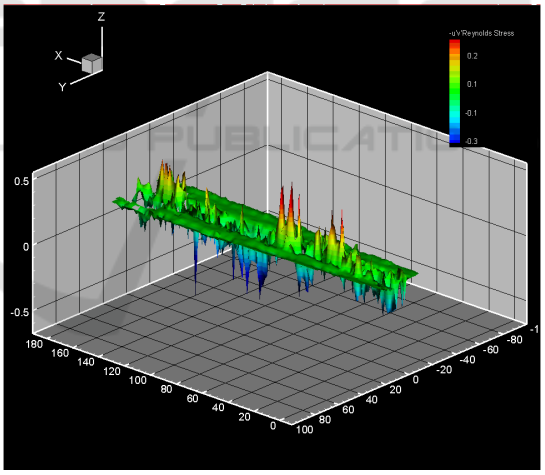

Figure 10: The Reynolds stress.

4 CONCLUSIONS

The turbulent flow field in a 50mm hydrocyclone was investigated with Particle Image Velocimetry. 200 visualizations were averaged and analyzed. Results show the averaged velocity field is smoother and more convenient for comprehending while the instantaneous velocity field is less distorted by the averaging process. Both the axial and radial velocity

components peak in the central area of the hydrocyclone. But for radial velocity, it varies between inward and outward from top to bottom, not exclusively inward in the cone section. For the secondary flow pattern, it is found that the secondary vortexes exist in the transition area of inner spiral flow and outer spiral flow, where higher vorticity is located. Turbulent intensity and Reynolds shear stress is also calculated from the two velocity components with time series. It is made clear that the central area is where the turbulence is strongest. And the maximum radial turbulence intensity exists in the vicinity of vortex finder tip, while maximum axial turbulence intensity exists in the lower cone section with transition of flow.

REFERENCES

Bergstrom, J., & Vomhoff, H., (2007). Experimental hydrocyclone flow field studies. *Separation and Purification Technology*, *53*, 8-20.

Lim, E. W. C., Chen, Y. R., Wang, C. H., & Wu, R. M., (2010). Experimental and computational studies of multiphase hydrodynamics in a hydrocyclone separator system. *Chemical Engineering Science*, *65*, 6415-6424.

Luo, Q., Deng, C., Xu, J. R. Yu, L. X., & Xiong, G. G., (1989). Comparison of the performance of water-sealed and commercial hydrocyclones. *International Journal of Mineral Processing*, 25, 297-310.

Marins, L. P. M., Duarte, D. G., Loureiro, J. B. R., Moraes, C. A. C., & Freire, A. P. S., (2010). LDA and PIV characterization of the flow in a hydrocyclone without an air-core. *Journal of Petroleum Science and Engineering*, *70*, 168-176.

Wong, W. O., Wang, X. W., & Zhou, Y., (2007). Turbulent flow structure in a cylinder-on-cone cyclone. *Journal of Fluids Engineering*, *129*, 1179-1185.

Yang, Q., Wang, H. L., Wang, J. G., Li, Z. M., & Liu, Y., (2011). The coordinated relationship between vortex finder parameters and performance of hydrocyclones for separating light dispersed phase. *Separation and Purification Technology*, *79*, 310-320.

Zhang, Y. H., Liu, Y., Qian, P., & Wang, H. L., (2009). Experimental Investigation of a Minihydrocyclone. *Chemical Engineering & Technology*, *32*, 1274-1279.

Zheng, Y., Liu, Z. L., Jiao, J. Y., Zhang, Q. K., & Jia, L. F., 2006. Investigation of turbulence characteristics in a gas cyclone by stereoscopic PIV. *Aiche Journal*, *52*, 4150-4160.